Spatial propagation of high-density excitons localized at a stacking disorder plane in BiI_3

H. Kondo,* H. Mino, I. Akai, and T. Karasawa
Department of Physics, Graduate School of Science, Osaka City University, Sumiyoshi-ku, Osaka 558, Japan
(Received 19 February 1998; revised manuscript received 17 August 1998)

We study spatial behavior of heavily excited excitons localized at a two-dimensional space of a specific stacking fault interface in a layered crystal BiI_3. Pump-and-probe absorption and resonant luminescence spectra of the exciton states were measured with an intense nanosecond laser not only at the exciting laser spot but at distant points from the exciting spot by applying space-resolved spectroscopy methods. The blueshift proportional to the exciton density was clearly observed on the probe absorption spectra even at the distant points due to high-density excitons flowing out from the exciting spot. The resonant luminescence also shows the spectral change and anomalous spatial expansion depending on the excitation density. The spatial distributions of the energy shift on the probe absorption and the luminescence intensity were analyzed on the basis of a two-dimensional exciton-flow model with dissipation processes. The analysis suggests the existence of an efficient in-phase motion of the exciton polaritons at high density. The results are discussed in terms of a new phase of the interacting high-density exciton-polariton system. [S0163-1829(98)05344-2]

I. INTRODUCTION

The nonlinearity of optical responses around the band-gap energy in semiconductors provides many interesting physical descriptions. One of the origins of nonlinear optical responses in materials is a virtual excitation of electronic states due to coherent multiphoton transition between the electronic energy levels by intense light field; the other is the many-body effect among really photoexcited electrons and holes. The optical Stark effect observed in nearly resonant energy region with respect to exciton states in semiconductors is one of the typical nonlinear optical responses due to the virtual excitation.[1] On the other hand, various phenomena due to the many-body effects in excited electronic systems have been found in GaAs crystals and in quantum-well (QW's) structures of GaAs/Al-Ga-As.[2–5] In these works the density-dependent spectral changes in absorption lines of excitons, i.e., the shifts of the transition energies, spectral line broadenings, and changes in oscillator strengths, have been discussed in terms of the phase-space filling, and screening in a dielectric exciton gas. In addition, the influence of many-body effects on the relaxation process of the excited states has been investigated by examining the time-correlated degenerate-four-wave-mixing (DFWM) signals with an ultrashort pulse laser.[6] In principle, the well-defined exciton states extend in whole in a perfect crystal. Therefore, in the excited-state physics not only relaxation processes in the time domain but also spatial transport or expansion of exciton after the photoexcitation are significant. In fact, the spatial behavior of excitons have been studied in terms of diffusive expansion in a few bulk semiconductors and GaAs-QW's by space-resolved measurements of luminescence,[7–9] by analyzing the spectral line shape,[10] and by using a nonlinear optical technique.[11] Furthermore, density dependence of spatial expansion and temporal behavior of excitons and photoexcited carriers in QW's has been examined.[9,12,13] In Refs. 12 and 13, spatial behavior of excited electrons at high density has been measured by the pump-probe method, where the increase of the diffusion coefficient is attributed to a driving force by a phonon wind.

In contrast with the diffusive process, the spatial expansion of excitons at an extremely low temperature has been thought to be the propagation in a polariton mode, and the propagation velocity of polaritons in GaAs, CuCl, and molecular crystals have been measured by the time-of-flight method and space-resolved measurements using short pulse lasers.[14–17] However, in order to detect the penetrated light pulse through crystals near the exciton resonance, specimens would have to be made extremely thin because of very large extinction coefficients. Thin crystals or quantum wells cannot, however, avoid the influence of roughness at interfaces and of imperfection in crystals. Therefore, it is difficult to distinguish the intrinsic properties of excitons in perfect crystals from extrinsic natures.

Subsequently, a new phase or a condensed state of weakly interacting boson systems have attracted much attention from the viewpoint of coherent and incoherent motions on the basis of the experimental observation of spatial behavior in neutral atom and exciton systems. In Cu_2O, an experimental study of exciton transport has been discussed in terms of excitonic superfluidity,[18,19] where it was reported that the ballistic exciton transport has a velocity close to the sound velocity asymptotically with increasing excitation density. This phenomenon has been treated theoretically with controversial discussion.[20–22] Therefore, it is interesting how exciton transport phenomena are affected by the excitation density. Experimentally, a system in which high-quality crystallization is realized and excitons can propagate without serious dissipation is required for such investigation.

An exciton system excited at a stacking fault interface in BiI_3 would satisfy the above requirements. Figure 1(a) shows a typical absorption spectrum below a bulk indirect exciton edge in BiI_3. A very sharp line series denoted by **P**, **Q**, **R**, **S**, and **T** from the high-energy side appears depending on samples.[23,24] Since the **P** line appears independently of the other lines, the origin of the **P** line has been attributed to some polytypic stacking disorder[25] or some localized state.[26] The absorption lines **Q**, **R**, **S**, and **T** have been ascribed to the exciton transitions perturbed by a specific stacking fault, which have been called stacking fault excitons

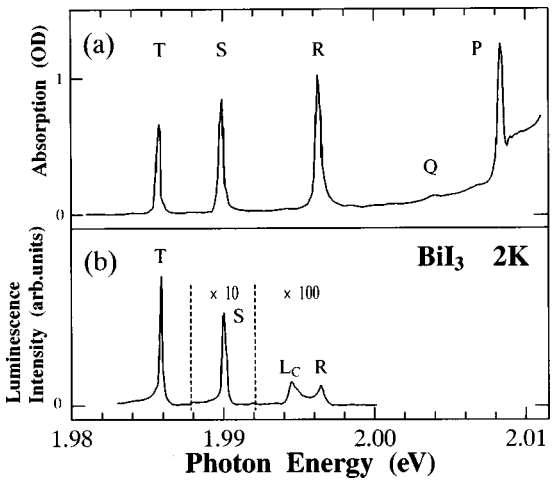

FIG. 1. (a) Absorption and (b) luminescence spectra of the SFE's in BiI_3 at 2 K. *Q*, *R*, *S*, and *T* in (a) are the SFE states. *P* is due to another stacking disorder origin. The sharp spectral peaks in (b) just at the SFE states are corresponding resonant luminescence; L_C is the luminescence from the indirect exciton state associated with phonon *C*.

(SFE's).[23,24,26] The SFE states are characterized by very large oscillator strengths, and strong Coulomb coupling, namely, a large binding energy. The SFE's show intense resonant luminescence. In Fig. 1(b), a typical luminescence spectrum is shown for the excitation at a band to band transition energy. The luminescence lines have zero Stokes shifts and have a line shape as sharp as the absorption ones; the luminescence band L_C is the phonon side band of the bulk indirect exciton.[27] The intensity of the SFE luminescence becomes stronger by more than one order of magnitude from *R* to *S* and from *S* to *T* as seen in the figure, which has been explained by an efficient cascade-type relaxation process among these states.[28] On account of the cascade relaxation, the population of the lowest lying *T* exciton becomes largest. As a result, the *T* state has a relatively long decay time constant 0.8 ns.[28] Subsequently, the *T* luminescence shows a high quantum efficiency very close to unity, which was confirmed from the measurements of photocalorimetric spectra.[29] The results of zero Stokes shift luminescence and extremely high quantum efficiency in SFE states indicate the realization of a defect-free interface of the stacking fault plane at which the dissipation processes for the excitons are significantly suppressed.

In the stacking fault plane, the translational symmetry is maintained in the macroscopic size of at smallest several hundreds micrometer and allows a quasi-two-dimensional motion for the center-of-mass motion of the SFE's. Kawai *et al.* reported that the resonant luminescence of SFE's expands much more widely along the stacking fault plane when the sample is excited with a focused laser spot of a very small size in area.[30] The temporal behavior of the spatially expanding SFE's has also been studied by the time-of-flight measurements.[31] It turned out that the observed propagation velocity 6×10^8 cm/s of the SFE is so rapid that the polariton picture is suitable. Then, it is not acceptable to attribute the propagation mechanism to the diffusive process which has been widely accepted for the propagation mechanism in other exciton systems in typical semiconductors. Furthermore, it was found from the DFWM measurements in this system that the phase relaxation of the SFE states has a fairly long time constant $\sim$40 ps which is longer than those observed usually in other exciton systems.[32] This also implies that this exciton system has large spatial coherency. These results show evidently that the SFE states construct a well-defined energy band in the *k* space.

The features of large binding energy and long lifetime of SFE states allow us to investigate high-density effects and nonlinear responses. In fact, the SFE system shows obvious nonlinear responses for intense laser excitation. The intense excitation effects on the SFE's were reviewed in detail in Ref. 33. The optical Stark effect induced by intense light field was observed in this system, indicating that our exciton system has a large dipole moment.[34,35] On the other hand, the real excitation effects on this system show that the increase in the exciton density brings about line broadening and peak-energy shifts of absorption lines to the higher energy side. The high density effect, however, brings about only slight decrease in the integrated intensities of the absorption lines. It means that the oscillator strength does not show obvious decrease. Schmitt-Rink *et al.* showed that a blueshift on an exciton transition energy takes place due to high-density effects especially in a two-dimensional exciton system.[5] In the previous paper,[33] we discussed that the peak-energy shift in proportion to the exciton density would be one of the features in a two-dimensional exciton system.

In our SFE system, it can evidently be said that the exciton center-of-mass motion is confined two dimensionally at the stacking fault plane, and the oscillator strength and the binding energy are fairly large. These features lead to the conclusion that the SFE's are stable even under the high-density condition. Furthermore, from the experimental point of view, the two-dimensional confinement, the high efficiency of the spatial transport, and the almost unity quantum yield of the luminescence would make the quantitative analysis of the exciton motion along the stacking fault plane much simple. Thus, we are very interested in the spatial behavior of the SFE's at high density.

In this paper, we present experimental results of dynamical processes of the SFE's in BiI_3 in real space under the intense laser excitation using space-resolved measurements.

II. EXPERIMENTAL METHODS

BiI_3 single crystals were prepared by the vapor-growth method. Since the appearance of the SFE transitions depends on samples,[30] the samples having uniform intensity distribution of the SFE transition lines along the sample plane and sharp spectral profiles of absorption and resonant luminescence lines of the SFE were selected. The samples were immersed in a superfluid liquid-helium bath and the measurements were performed at 2 K.

For the light source to excite heavily the SFE states, a dye laser (Molectron: DL-12) with the spectral width less than 0.1 meV and the time duration of $\sim$6 ns pumped by a pulsed N_2 laser (Molectron: UV-14) was used with a repetition rate $\sim$10 Hz; rhodamine B dye of which fluorescence covers the spectral region of the SFE transition lines was used. For all

measurements, unless otherwise stated, the wavelength of the laser was tuned to the **S** absorption line. The output power of the laser was 2×10^{-6} J/pulse; this value was rather weakened at the sample surface put into the quartz cell of the cryostat through many optical elements.

For space-resolved measurements, the laser beam was focused by a lens on the sample surface. The spatial profile of the focused laser beam on the sample surface was nearly the Gaussian shape with 56 μm in full width at half maximum. In order to obtain a high spectral resolution, we used a double-grating monochromator (Jobin Yvon: U-1000). The signal was averaged by a boxcar integrator (NF Circuit Design Block: BX-531).

A. Observation of the space-resolved pump-probe absorption spectra

The absorption spectra were measured by the pump-probe method both in the usual manner and in a space-resolved regime. The laser beam was used for the pump light, and the fluorescence component from the dye cell was used for the probe light. The probe light having the same time duration 6 ns as that of the dye laser pulse was coincided with the pump light on the sample surface through an optical delay path.

For the usual pump-probe method, the pump light was defocused in order to irradiate the sample surface uniformly and not to be influenced by the spatial distribution of the pump light intensity, and the probe light was focused to a smaller spot size in part of the surface irradiated by the pump light; this experimental condition is named ''the uniform excitation condition'' in the following. In this work, in addition to the above-mentioned geometry, we tried to focus separately the pump and probe lights to each spot of about 60 μm in diameter on the sample surface, named ''the space-resolved pump-probe method.'' Changing the distance r between the pump and the probe beam positions on the sample by adjusting finely micrometers at the focusing lenses, and varying the pump light intensity, we measured change in the absorption spectra. In order to vary the pump light intensity, the neutral density filters were inserted into the pump beam path. This method gives a spatial resolution up to $\sim$50 μm. The pump light passing through the sample was cut off by an aperture, and only the probe light was led to the monochromator.

In order to detect the very small change in absorption spectra accurately, difference spectra between pumped and unpumped absorption were measured by an alternative detection of the probe light in accordance with the pump light timing by using a chopper for the pump light and the boxcar integrator with an alternative mode. More details are described in our previous papers.[36,37]

B. Observation of the space-resolved luminescence spectra under the high-density excitation

In order to obtain the space-resolved luminescence spectra under the high-density excitation, the exciting laser light was focused to a small spot of $\sim$50 μm in diameter on the sample surface. The image of the luminescence excited by the laser was enlarged by about ten times with an anastigmatic camera lens and was projected onto a screen. The screen was set and was finely adjustable on a *XYZ* stage; the *Z* axis was set to be parallel to the optical axis of the camera lens. A glass fiber of 200 μm in diameter with a light-focusing fiber-guide (Nippon Sheet Glass Co., Ltd.: SELFOC Micro Lens) at the terminal was attached to a pin hole on the screen. The pin hole and the light-focusing fiber-guide efficiently picked up a very small part of the finely focused luminescence image within $\sim$300 μm in diameter. The glass fiber led the luminescence light to the monochromator with very high efficiency and without any deformation of the spectral shape within the wavelength range concerned. More details are also described in our previous papers.[30,38] The spatial resolution of this system reached up to 30 μm. For the space-resolved spectra, we scanned wavelengths of the monochromator at each position on the sample. For the spatial distribution of the luminescence intensity, we scanned the position of the screen along the *X* or *Y* axes at each wavelength.

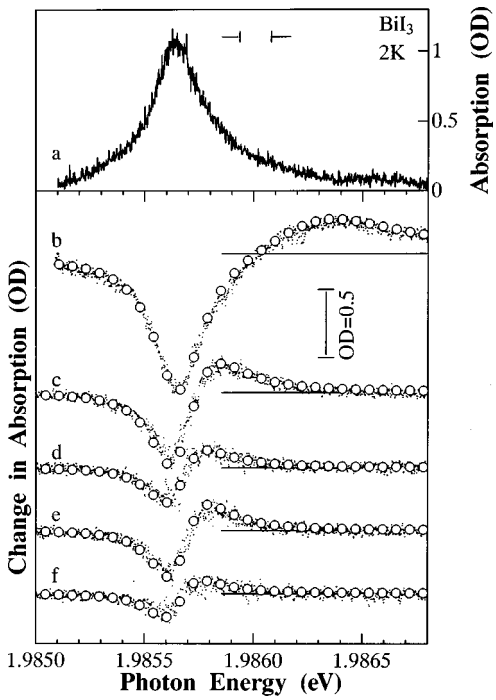

FIG. 2. Curve *a* absorption spectrum of the *T* line in BiI_3 at 2 K by only the probe light. Curves *b*, *c*, and *d* difference spectra of the *T* line, i.e., those of the subtracted pumped ones by the umpumped ones, for the maximum incident laser intensity I_L at $r=0$, $r=0.15$ mm, and $r=0.25$ mm, respectively. Curves *e* and *f* at $r=0.15$ mm for the intensities $I_L/2$, and $I_L/4$, respectively. The uppermost vertical split shows the slit width. Open circles exhibit each calculated difference spectrum from Eqs. (2) and (3).

III. RESULTS AND DISCUSSION

A. Space-resolved absorption spectra due to the pump-probe method

Figure 2 shows the change in absorption by the space-resolved pump-probe method on the *T* line in BiI_3 at 2 K in various pumping power at various distances; spectrum **a** is the *T* line absorption by only the probe light. The spectrum shows the peak absorption intensity to be $\sim$1 in O.D. and the linewidth (full width at half maximum: FWHM) to be $\sim$0.3 meV. The spectra *b*–*f* (dots) show difference spectra

of the probe absorption from unpumped ones; for all spectra, the pumping laser wavelength was tuned to the higher lying S line. The spectral change takes place most remarkably at the pump spot ($r=0$) as shown by spectrum b in the figure; here, the incident laser intensity was the maximum one of 8.0×10^{-8} J/pulse for the pump-probe measurements; this value is limited by the maximum power which does not damage the sample and corresponds to 1.8×10^{-3} J/cm^2/pulse (I_L) at the sample surface by taking the focused laser-spot size and all the reduction factors along the optical path into account. The difference spectra are characterized by the peak energy shift to the high-energy side, line broadening, and the reduction in the absorption cross section. The change does occur not only at the pumping position but also at the positions away from the pump spot by $r=0.15$ mm (spectrum **c**); the obvious change was detected even at the position by $r=0.25$ mm (spectrum d) for the maximum excitation intensity I_L. At a distance $r=0.15$ mm, the change becomes larger with increasing excitation intensity from $I_L/4$ to $I_L/2$ and I_L as seen in spectra f, e, and c in order.

It might be said that a lattice-temperature rise due to the irradiation of the intense pump light brings about some spectral change.[39] It should take a certain time to detect the spectral change due to the thermal effect transported, at the fastest, at the sound velocity to a distant point from the exciting laser spot. The previously obtained sound velocity $\sim10^5$ cm/s in this material[40] gives at the shortest a transport time $\sim10^{-7}$ s of the heat between pump and probe points, which is much longer than the pump and probe light pulse duration of 6×10^{-9} s. As mentioned in Sec. II, the pump and probe lights were coincided to arrive at the same time on the sample surface within the pulse duration. In fact, the spectral change was not detected when the relative time difference between the two exceeded the duration. Consequently, the thermal effect does not explain the spectral change. Thus, this spectral change is brought about by the really excited high-density excitons propagating with a velocity much faster than phonons. Then, we regard the spectral change as an effect due to the high-density excitons. We analyze the nonlinear spectral responses due to the high-density excitons in detail as follows.

In general, the absorption spectrum of the homogeneously broadened exciton state interacting weakly with other systems is expressed by an asymmetric Lorentzian[41] as

$$\alpha_0(\hbar\omega)=\frac{a_0}{\pi}\frac{\Gamma_0/2+2A_0(\hbar\omega-E_0)}{(\hbar\omega-E_0)^2+(\Gamma_0/2)^2}, \tag{1}$$

where E_0 is the peak energy of the absorption line, Γ_0 being the line width (FWHM), A_0 being the degree of asymmetry, and a_0 being an absorption cross section proportional to the oscillator strength. The probe spectrum **a** can well be fit by Eq. (1) with the values $E_0=1.98564$ eV, $\Gamma_0=0.27$ meV; the width Γ_0 includes the homogeneous broadening and that from the apparatus function.[42]

When the SFE states are irradiated by the pump light, the absorption line changes its profile from $\alpha_0(\hbar\omega)$ in Eq. (1) to $\alpha_I(\hbar\omega)$ as

$$\alpha_I(\hbar\omega)=\frac{a_I}{\pi}\frac{(\Gamma_0+\Delta\Gamma)/2+2A_I[\hbar\omega-(E_0+\Delta E)]}{[\hbar\omega-(E_0+\Delta E)]^2+[(\Gamma_0+\Delta\Gamma)/2]^2}, \tag{2}$$

TABLE I. The best-fitting parameter values in Eqs. (2) and (3) for each difference spectrum of the **T** line in Figs. 4. b–f correspond to the curves b–f in Fig. 4, respectively.

	Distance r (mm)	Laser intensity	ΔE (meV)	$\Delta\Gamma$ (meV)	α_I/α_0	A_I
b	0	I_L	0.61	0.47	0.74	0.25
c	0.15	I_L	0.12	0.099	0.89	0.04
d	0.25	I_L	0.050	0.037	0.96	0.01
e	0.15	$I_L/2$	0.072	0.042	0.95	0.02
f	0.15	$I_L/4$	0.031	0.020	0.97	0.01

where ΔE and $\Delta\Gamma$ are the amount of the change in each quantity for the heavy excitation; a_I and A_I being the individual quantities concerned under the condition. The difference spectra are given by

$$\Delta\alpha_I(\hbar\omega)=\alpha_I(\hbar\omega)-\alpha_0(\hbar\omega). \tag{3}$$

The calculated spectra for various excitation intensities at various distant positions well reproduce the experimental data (dots) as shown in Fig. 2 by open circles. Each fitting parameter value is listed in Table I. It is confirmed that the shift ΔE and the broadening $\Delta\Gamma$ increase with increasing incident laser intensity and with reducing distance. At $r=0$, the large blueshift, remarkable broadening, and the significant reduction of the absorption cross section by 26% take place.

The spectral change brought about by the intense laser excitation has been understood by the high-density effects and the optical Stark effects. For the high-density effects, as mentioned in Sec. I, Pauli's repulsion and Coulomb screening dominate these effects which give the energy shift, especially on two-dimensional exciton systems. In our SFE system, the origins of the spectral change have been classified into two: field-induced effects, namely, the optical Stark effects, and mutual interaction due to really excited high-density excitons, i.e., high-density effects. In previous works, we have shown that the optical Stark effects bring about laser-frequency-dependent transition-energy shifts and a serious reduction of the absorption cross section,[34,35] and the high-density effects bring about spectral blueshifts without remarkable reduction of the cross section.[33] In the space-resolved regime in this work, at $r=0$, the remarkable shift and serious reduction of the cross section were observed again. Then, the cross section reduction can be regarded as the optical Stark effects. On the contrary, the reduction rates of the cross section at the finite distant points ($r\neq0$) are fairly small. Since the electric field of the pump laser light does not exist at $r\neq0$, the optical Stark effect does not take place. Then, the blueshift at $r\neq0$ originates from the high-density effects. Furthermore, the amount of the energy shift at $r=0$ is one order of magnitude larger than that estimated for the optical Stark effect from the extrapolation of the off-resonance excitation in the previous paper.[34] As a result, the shifts, even at $r=0$, are attributed to the high-density effects. Consequently, the energy shift which can be resolved from the probe spectra with high accuracy is available as a simple and significant index for the high-density effects as treated later. Correspondingly, the broadening of the line shape is

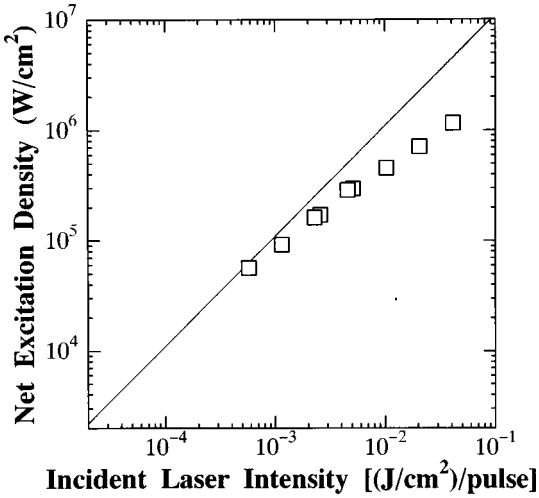

FIG. 3. Calibration for the net excitation density vs incident laser intensity (see text). The straight line shows the linear correspondence.

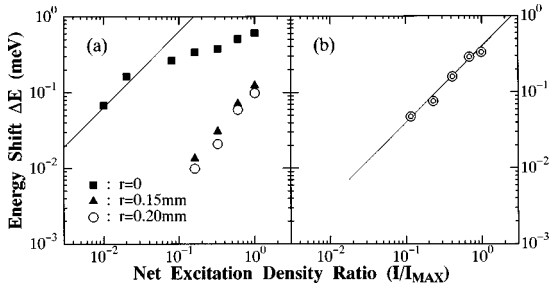

FIG. 4. Peak energy shift of the T line as a function of the excitation density (a) at various distances in the space-resolved regime, and (b) for the uniform excitation condition (see text in details). The net excitation densities in (a) and (b) are depicted by the ratios of the excitation densities to the maximum ones, respectively. The straight lines in (b) as well as in (a) indicate the linear dependence of the ΔE for the net excitation density; for that in (a), the net excitation density is shifted for the absolute value to coincide with (b).

considered to originate from homogeneous lifetime broadening due to the collision with high-density excitons. Here, the lifetime means the dephasing time of the exciton state in the true sense. In contrast with the dephasing time, we use ''decay time'' given from the temporal change in the luminescence intensity as a time constant of the radiatively or nonradiatively dissipating excitons from their band. The dephasing time will be discussed later in connection with exciton mean-free-path lengths.

In order to obtain the quantitative change in the spectra for the exciton density, the true exciton density must be evaluated for the exciting laser light intensity. The exciton density is proportional to the photon number absorbed in the sample within its lifetime. In general, the absorbed photon number is not proportional to the incident photon number because of the change in the absorption intensity under the high-density excitation. In this work, the incident laser light is tuned to the peak of the higher lying absorption line S. When the S line is excited heavily, it shows also the peak shift and line broadening in the same manner as in **T**. The laser light has a sufficiently narrow wavelength width compared with the absorption linewidth of the S line, and the wavelength of the laser light was fixed to the usual absorption peak position of the S line. For the calibration of the absorbed photon number under the condition, the transmittance and reflectance of the exciting laser light on the sample were measured for various incident laser intensities. Thus, we obtained the true absorbed light intensity, i.e., net excitation density as a function of the incident laser intensity as shown in Fig. 3, here the straight line shows the linear relation. As expected, the net excitation density becomes not to be proportional to the incident laser intensity in the higher intensity region. Hereafter, we use the net excitation density I in exchange for the crude incident laser intensity.

Figure 4(a) shows the energy shift ΔE of the T line at various positions with distance r as a function of the net excitation density ratio I/I_{MAX}, where I_{MAX} is the maximum net excitation density corresponding to I_L; $I_{\mathrm{MAX}}=1.3\times10^5$ W/cm^2 in the space-resolved regime. The energy shift $\Delta E(0)$ at the pumping point ($r=0$) tends to saturate with increasing density I. However, ΔE for $r\neq0$ increases superlinearly with the increase of I, and the increasing rate of ΔE becomes large with the distance. The observed energy shift at $r\neq0$ evidently shows the existence of spatial expansion of the high-density excitons from the exciting laser spot. Furthermore, the saturation phenomenon of the excitation-density dependence of the energy shift at $r=0$ is understood by the same origin of the spatial expansion effect as discussed later.

In order to clarify the spectral change for the exciton density, the energy shift for the excitation density was also measured under the uniform excitation condition and is shown in Fig. 4(b); the pump-light spot size is tuned to ~2 mm in diameter on the sample surface. In this case, the maximum density I_{MAX} was reduced to be $\sim7.5\times10^3$ W/cm^2 because of the larger spot size, although the crude incident laser intensity was increased. The shift ΔE is exactly proportional to the net excitation density I. The straight line in (b) indicates the linear relation; the straight line in (a) is the same one as in (b) and is depicted for the scale of the net excitation density to coincide with that in (b) in absolute value. Under this uniform excitation condition, the photocreated excitons exist with a spatially uniform density in the much smaller area of the probe-light spot of ~60 μm, because spatial expansion of the excitons plays a role to make the density homogeneous. For the exciton density under the pulsed excitation, one needs to know the exciton decay time. The decay time of the T exciton, which is the longest in the SFE states, has been observed to be 0.8 ns from the measurement of the temporal behavior of the resonant luminescence.[28] Since the exciting laser pulse duration is about 6 ns much longer than the exciton decay time, it can be regarded that the excitation condition is stationary. The stationary condition leads straightforwardly to the relation that the exciton density is proportional to the net excitation density I. As a result, it is concluded that the energy shift is proportional to the exciton density. Hereafter, we introduce the local exciton density as the exciton density of a function of the distance r. According to the above-mentioned result, the shift ΔE at each position r in the space-resolved regime shown in Fig. 4(a) is an amount proportional to the local exciton density n at r as

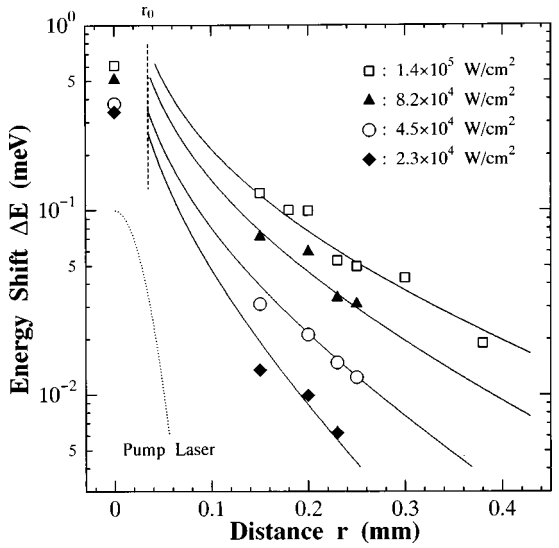

FIG. 5. Peak energy shift of the T line as a function of distance r between pump and probe spots for various excitation densities. Solid lines are best-fitted lines by Eq. (5) for each excitation density; the parameter values of d in Eq. (5) are 0.30, 0.22, 0.16, and 0.10 mm, respectively, from higher excitation densities. The vertical broken line denotes the effective pump spot radius r_0. The dotted curve denotes the observed pump laser profile.

$$\Delta E(r) \propto n(r). \tag{4}$$

Figure 5 shows the shift ΔE for various net excitation density as a function of the distance r under the space-resolved condition; each exciting power indicated in the figure is already corrected as the net excitation density in the manner described in Fig. 3. Accordingly, Fig. 5 can be regarded as the spatial distribution of the exciton density for each excitation density. When the excitation density increases, the spatial gradient of the exciton density with respect to the distance decreases in absolute value indicating the additional expansion of the higher density excitons from the exciting spot.

As reported in the previous work concerning a time- and space-resolved luminescence measurement, it was found that the propagation velocity of the exciton is so fast that the exciton motion in the real space cannot be explained only by the diffusive process but by the polaritonlike one.[31] The spatial distribution of the high-density excitons shown in Fig. 5 indicates that the high-density excitons expand in the range of ~ 0.2 mm in radius from the exciting spot. By considering their lifetime of 0.8 ns, it fails to treat the propagation mechanism as diffusive because the obtained parameter values provide an unreasonably large diffusion constant.

So, we try to deal with the spatial distribution of the high-density excitons as a two-dimensional exciton flow. It is assumed that the excitons flow out in the radial direction symmetrically with respect to the pump spot and their flow decreases exponentially with distance r. Then, the flow density of the excitons $u(r)$ is proportional to the quantities as

$$u(r) \propto \frac{\exp(-r/d)}{r}, \tag{5}$$

where d is a spatial decay length. Now, the exciton density $n(r)$ has a relation to the flow density $u(r)$ as follows:

$$u(r) = \langle v \rangle n(r), \tag{6}$$

where $\langle v \rangle$ is the mean velocity of the exciton flow, namely the drift velocity. For simplicity, it is assumed that the drift velocity $\langle v \rangle$ does not depend on the distance r. Subsequently, the exciton density $n(r)$ is proportional to $u(r)$. The expansion of the spatial distribution of the excitons for each excitation density can be well fit by Eq. (5) with only one parameter d; the values of d for every excitation are 0.30, 0.22, 0.16, and 0.10 mm from higher excitation densities, respectively. The solid lines in Fig. 5 represent the best fits of Eq. (5) for each excitation density I. Here, the fitting was done in the region outside the exciting spot characterized by a radius r_0, because Eq. (5) cannot be applied inside the spot in which excitons are supplied by the laser light. The value of parameter d increases with increasing net excitation density as clearly seen in the figure.

Furthermore, in order to examine the decay processes of the high-density excitons, we evaluate a total number of the excitons in the whole space by integrating the local exciton density for each excitation density. Then, the stationary total exciton number N is given as

$$N = \int n(\vec{r}) d\vec{r}. \tag{7}$$

For our system, the integral region is restricted in the two-dimensional space on the stacking fault plane. Since the local exciton density $n(r)$ is proportional to the energy shift $\Delta E(r)$ at each point as indicated in Eq. (4), $\Delta E(r)$ is substituted for $n(r)$ in Eq. (7). In order to perform the calculation of Eq. (7), the integrand $\Delta E(r)$ is divided to two parts: $\Delta E(r)$ within r_0 of the effective pump spot radius, and $\Delta E(r)$ which has the analytical form of Eq. (5) in the region with larger radius r than r_0. The amount of $\Delta E(r)$ within the radius r_0 is taken to be a constant value $\Delta E(0)$. Consequently, we obtain the total number of excitons in proportion to the next quantity using the ''integrated energy shift'' as

$$N \propto \pi r_0^2 \Delta E(0) + 2\pi \int_{r_0}^{\infty} \Delta E(r) r \, dr. \tag{8}$$

In Eq. (8), the first term expresses the average number in the pump spot, and the second term comes from the flowing-out component from the pump spot. Figure 6 shows the integrated energy shifts as a function of the net excitation density. The integrated energy shift, namely the total exciton number N, is proportional to the net excitation density as can be seen in the figure.

The relaxation of the total exciton number N is generally given by the next rate equation as

$$\frac{dN}{dt} = -\frac{N}{\tau_{\mathrm{ex}}} + I_n(t), \tag{9}$$

where $I_n(t)$ is the supply of excitons by the pump light and is proportional to the net excitation density, τ_{ex} being the decay time of the exciton in the whole space. From the stationary condition, the left-hand side of Eq. (9) becomes zero. Then, we obtain

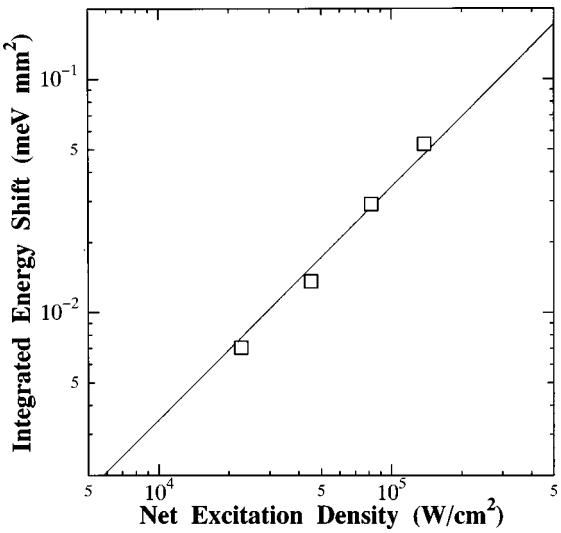

FIG. 6. Integrated energy shift of the T line vs net excitation density [see text and Eq. (8)]. Straight line denotes the linear relation.

$$N = I_n \tau_{\mathrm{ex}}. \tag{10}$$

Since the stationary total exciton number N is proportional to the net excitation density as seen in Fig. 6, it is concluded that the exciton decay time τ_{ex} at high density has a constant value independent of the excitation density. By considering the luminescence quantum efficiency to be unity for the weak excitation, the result of the constant decay time for excitation density indicates that heavily excited excitons have also the same high quantum efficiency. This means that they decay radiatively from the band bottom at $k \simeq 0$ of the lowest T state without any nonradiative decay to the free carriers and to other trapping or relaxed states everywhere they do. Accordingly, the decrease of the absolute value of the spatial gradient of the local exciton density with increasing excitation density is not attributed to the increase of the exciton decay time but to the increase of the drift velocity. The drift velocity of the exciton flow $\langle v \rangle$ is evaluated from the next equation and the fitting value d in Fig. 5,

$$d = \langle v \rangle \tau_{\mathrm{ex}}. \tag{11}$$

Since the exciton decay time τ_{ex} has been obtained to be 0.8 ns at low density limit and is assumed to be constant for the excitation density, the drift velocity $\langle v \rangle$ is evaluated from 1×10^7 cm/s to 4×10^7 cm/s for the lowest to the highest excitation densities in Fig. 5. Thus, the drift velocity increases with increasing excitation density.

B. Space-resolved luminescence spectra under the high-density excitation

The resonant luminescence of T was examined in detail under the high density excitation at the S state in the space-resolved regime. Space-resolved resonant luminescence spectra under different excitation densities are shown in Fig. 7 for distances $r = 0$ (a), and $r = 0.075$ mm (b). For comparison, a transmittance spectrum of the T line without pump light is also shown in Fig. 7(a). The luminescence peak shifts to the high-energy side for high-density excitation. The amount of the peak shifts is smaller than that in the pump-probe absorption for the same excitation density; the densities are 2.3×10^5 W/cm^2 for spectra A and 7.5×10^4 W/cm^2 for spectra B. For an excitation density $\sim 2 \times 10^5$ W/cm^2, for example, the shift energy at $r = 0$ is about a half of that in the absorption spectrum. The reason for this is that in the luminescence spectra any radiative processes are superimposed including any energy relaxation processes via scattering and trapping. The spectral shapes at the exciting spot ($r = 0$) are symmetrical and more broadened for heavier excitation, but outside the exciting spot ($r = 0.075$ mm) the shapes have tails to the low-energy side. For the highest excitation density (spectrum A), the peak intensities at $r = 0$ and $r = 0.075$ mm does not change a great deal, although the spectral profiles differ from each other. When the excitation density is decreased, the decreasing rate of the luminescence intensity at $r = 0$ is smaller than that at $r = 0.075$ mm. The curious excitation density dependence of the luminescence intensity will be discussed in connection with integrated intensities over the whole area on the sample. For the spectral shape, it is considered that the broadening component comes from the lifetime broadening due to the scattering by the high-density excitons, or comes from the broadening due to temporally inhomogeneous excitation. At $r = 0$, the lifetime broadening would be predominant, because excitons supplied by exciting light bring about the broadening due to frequent scattering with each other. The low-energy tail at the distant point outside the exciting spot would be caused by any relaxation processes.

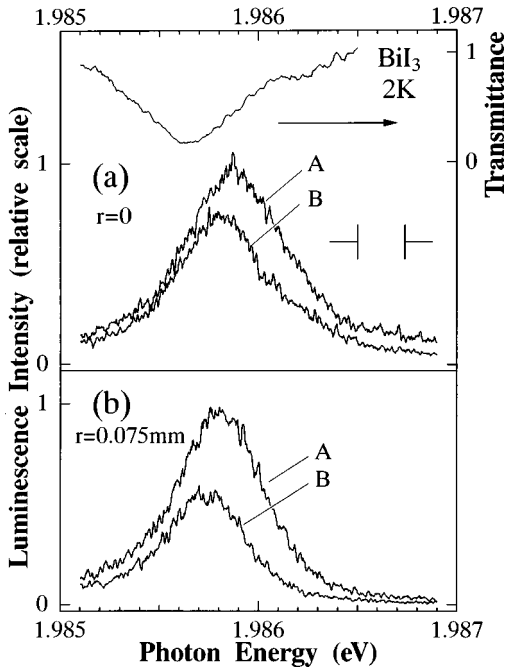

FIG. 7. Space-resolved luminescence spectra of the T line in BiI_3 at 2 K (a) at $r = 0$, and (b) at $r = 0.075$ mm for two different excitation densities: A 2.3×10^5 W/cm^2, and B 7.5×10^4 W/cm^2. The uppermost spectrum in (a) denotes the transmittance spectrum of the T line without pumping. The luminescence intensity scale is taken to be compared directly. The vertical split shows the slit width.

In order to know the spatial distribution of the T luminescence intensity in the whole spectral region, the luminescence intensity was measured as a function of distance r in a

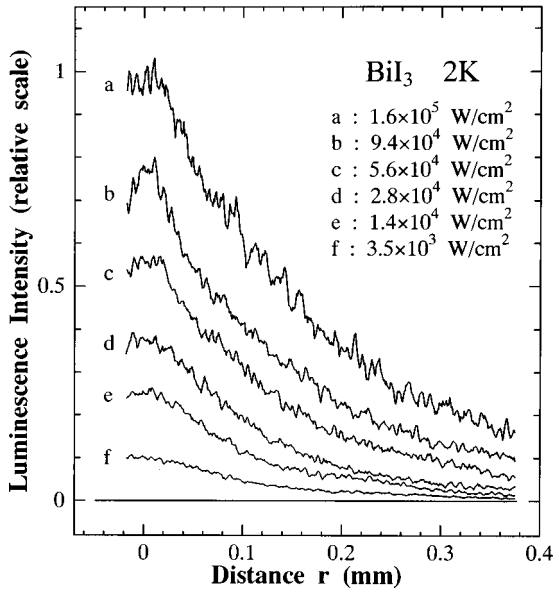

FIG. 8. Space-resolved luminescence intensity of the T line vs distance r for various excitation densities in the same scale.

radial direction; the intensity for every radial direction is symmetric with respect to the exciting point. Since the spectral profile of the T luminescence changes for the excitation density and the distance, the slit width was sufficiently widened to cover the whole spectral region of the T line for any excitation densities in order to obtain the whole T luminescence intensity. Thus, we defined the ''local luminescence intensity'' as the space-resolved luminescence intensity in the whole spectral region of the T line. Figure 8 shows the spatial distribution of the local luminescence intensity for various excitation densities. In this figure, each intensity is plotted in the same and linear scale. As expected, the luminescence expands more for higher excitation density into several tenths mm region. It should be noted that the increment of the intensity ratios at larger r with increasing excitation density becomes obviously larger than that at smaller r, that is, the higher the excitation density is increased, the more the luminescence expands.

Figure 9(a) shows the excitation-density dependence of the local luminescence intensity at $r=0$. The intensity has a clear tendency to saturate with the net excitation density. On the contrary, the intensity at larger r becomes to increase

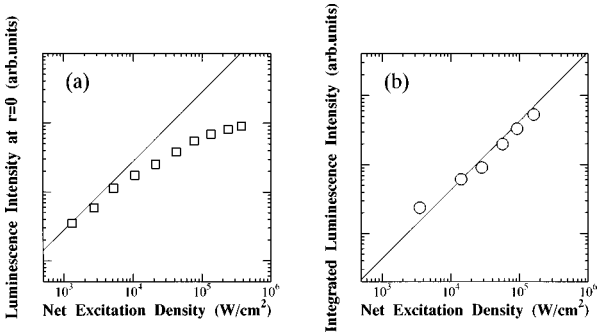

FIG. 9. (a) Luminescence intensity of the T line at $r=0$, and (b) the integrated luminescence intensity as a function of the net excitation density. Each straight line denotes the linear relation.

superlinearly for the net excitation density as also gauged from Fig. 8. As the total exciton number has been evaluated from the integration of the energy shift in the space-resolved pump-probe spectra, we obtain each integrated luminescence intensity for every respective excitation density integrating the intensity distribution over the whole area in the two-dimensional space.[43] Figure 9(b) shows thus obtained integrated luminescence intensity as a function of the net excitation density. The intensity is almost proportional to the net excitation density. This result implies that the luminescence quantum efficiency in the whole area does not change with increasing excitation density. Then, from the fact that the quantum efficiency of the T state is unity for weak excitation,[29] it can be said that the expanding excitons at high-density decay only through the radiative transition at somewhere along the stacking fault plane with unity quantum efficiency.

The time- and space-resolved measurements of the resonant luminescence under the weak excitation condition showed that the luminescence expands spatially as a ripple on the water surface,[31] that is, the expansion of a large majority of the SFE's is not diffusive but ballistic as a polariton mode. As shown in Figs. 8, and 9, the spatial expansion of the luminescence was certainly enhanced under the intense excitation. Thus, we infer that a ballistic flow mechanism predominates in the expansion of the SFE polaritons under the high-density excitation. So, in order to analyze the spatial distribution of the heavily excited luminescence, we assume that the exciton polaritons contributing to the luminescence flow out concentrically in the two-dimensional space from the exciting point.

This assumption leads to the result that the dissipationless flow decreases to the inverse of the radial distance $1/r$ with being propagated in the radial direction. Therefore, in order to clarify the spatial dissipation of the luminescence flow, we define the ''radial luminescence intensity'' $F(r)$ as the intensity integrated along the circle with radius r:

$$F(r)=\int_0^{2\pi} L(r)r\,d\theta=2\pi rL(r), \tag{12}$$

$L(r)$ being the local luminescence intensity at a position with distance r. Thus, we can treat the real-space distribution of the luminescence by the simple intensity $F(r)$ instead of $L(r)$.

Figure 10 shows the radial luminescence intensity for various excitation densities. If the decay time of the exciton were infinite, i.e., no dissipation process existed, the function $F(r)$ would be independent of r giving a horizontal line in Fig. 10. On the other hand, for the infinitesimal decay time, the exciton would not be propagated, and $F(r)$ would give only the spatial form of the luminescence source, i.e., the exciting laser profile. In practice, when the decay time τ_{ex} is a constant and finite value, and on the assumption that the velocity v of the exciton propagation along the radial direction is independent of r, $F(r)$ will decrease exponentially with r giving a straight line in the figure with a gradient $-1/\xi$:

$$F(r)\propto\exp(-r/\xi), \tag{13}$$

where the attenuation length ξ is given as

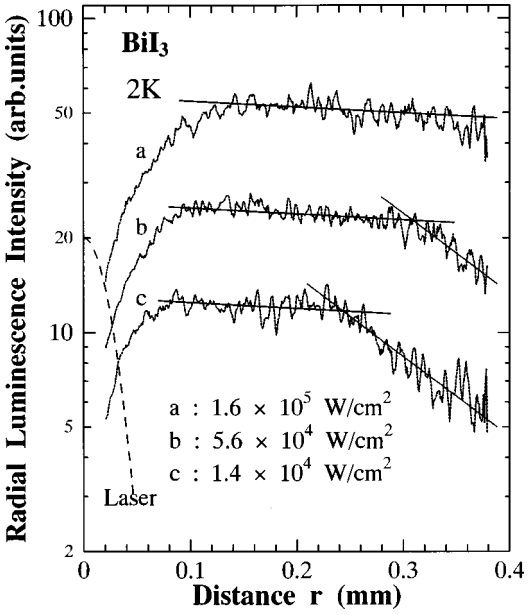

FIG. 10. Radial luminescence intensity vs distance r for various excitation densities (see text). The straight lines show the fit by Eq. (13) for the attenuating luminescence. The broken line is the exciting laser trace.

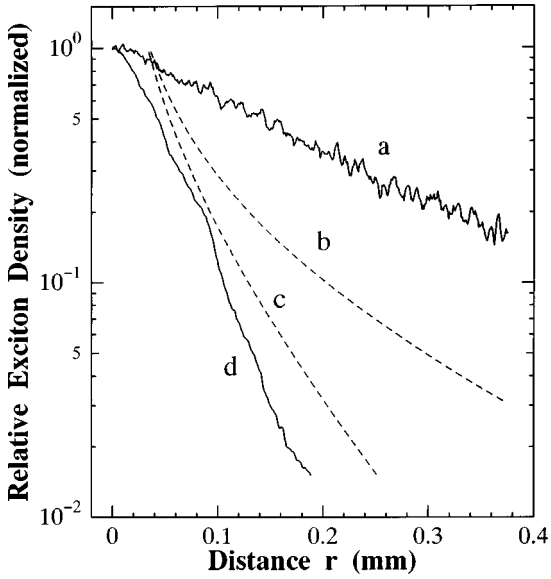

FIG. 11. Relative exciton density vs distance r. Curve a is that from the luminescence intensity of the T line, the same as trace **a** in Fig. 10. Curves b and c are that from the peak energy shift of the T line for different excitation densities, the same as the maximum and the minimum excitation densities in Fig. 7, respectively. Curve **d** is the trace of the luminescence intensity for the weak excitation limit.

$$\xi = v\,\tau_{\mathrm{ex}}. \tag{14}$$

As seen in Fig. 10, the profile $F(r)$ in the small r near the exciting spot shows a rise. For larger r than ~ 0.1 mm, $F(r)$ can be divided into two steps: the first step where it can be fit to an almost flat straight line with a small gradient in absolute value, and the second step with a large gradient in absolute value as shown in Fig. 10. The flat region is more lengthened with increasing excitation density. The gradient of each intensity is equal to each other for the various excitation densities. At larger r or for weaker excitation density, another attenuation process appears with a larger gradient in absolute value as also shown by the other lines in the figure. The rising component in the small r seems to grow with increasing excitation density beyond the exciting laser spot region; in the model the rise appears within the source region of the laser spot. Such a rising component suggests that nonluminescent transport processes exist in that area beyond the source region including the relaxation processes from the higher SFE level via the higher intraband state.

From the gradients of the attenuation processes in Fig. 10, we obtain two values for the attenuation length ξ: $\xi = 2.3$ and 0.17 mm for the small and large gradients, respectively. As discussed before, the decay time τ_{ex} in this system can be regarded to be constant in the whole area for any excitation density, i.e., $\tau_{\mathrm{ex}} = 0.8$ ns. Furthermore, by using the group velocity of the exciton polariton $v_g = 6 \times 10^8$ cm/s for the velocity v in Eq. (14), the attenuation length ξ is evaluated to be 4.8 mm. This value is close to that obtained from the small gradient line with a difference only by factor 2. This leads to the conclusion that the flat component in Fig. 10 predominantly comes from the exciton polaritons with the group velocity transported without suffering from serious scattering as also discussed in the next subsection. Subsequently, the large gradient component would exhibit the excitons experiencing scattering processes giving a smaller mean velocity.

C. Discussion

We have obtained the information on the spatial distribution of the SFE's at high density by intense laser excitation from the space-resolved transition spectra. However, the results show different aspects between the pump-probe absorption and the luminescence spectra. In this subsection, we discuss the mechanisms which govern the spatial expansion or transport of the excitons at high density comparing the results of the two kinds of experiments.

Figure 11 shows the spatial distribution of each exciton density in logarithmic scale; curve a is the T luminescence intensity excited with the maximum laser intensity, which is the same as curve a in Fig. 8, curves b and c are the peak energy shift of the pump-probe absorption, and are the same as the upper most and the lowest curves in Fig. 5, respectively, and curve d is the luminescence distribution in the low-density excitation regime, where a cw He-Cd laser with an average power of 50 mW was used for the exciting light source.[30] The heavily excited luminescence distribution a expands more largely than d for the weak excitation. We have described that the integrated luminescence intensity is in proportion to the excitation density as shown in Fig. 9(b), and the quantum efficiency of the luminescence is unity. From these results, the expansion of the spatial distribution of the luminescence intensity for the heavy excitation indicates that the ratio of the number of luminescent excitons at a position to that of the total excitons in the whole area changes depending on the excitation density. As readily understood, in curve d for the weak excitation limit, the local luminescence intensity is simply proportional to the exciton density at each

position. On the other hand, for the high-density excitation, the distribution of the local exciton density gives curve *b* as well as curve *c* in Fig. 11, since the peak energy shift is proportional to the local exciton density as mentioned before. However, luminescence distribution *a* is different from curve *b* of the local exciton density, although both of the excitation densities for *a* and *b* are almost equal. This discrepancy between their spatial distributions at high density implies that the local luminescence intensity is not proportional to the local exciton density, and the more the density increases, the more the ratio of the nonluminescent excitons at the position increases. This means that a fairly large portion of high-density excitons expand nonradiatively to the larger distant area, and emit light there resulting in curve *a*.

It can be said that the luminescence intensity is proportional to a number of the excitons at $k \simeq 0$ in the exciton band, from which the radiative transition can occur. On the other hand, the higher density excitation constructs the exciton population at larger k, which is responsible for the energy shift of the probe spectra and does not mainly contribute to the luminescence process. Consequently, the discrepancy of curve *a* from curve *b* comes from the increment of the exciton population at $k \neq 0$. Subsequently, the discrepancy of curve *b* from curve *d* is clearly understood as follows. The spatial distribution of the luminescence intensity under the weak excitation limit is determined by intrinsic propagation and dissipation mechanisms depending on the lattice temperature and the degree of completeness of the translational symmetry of the stacking-fault plane. On the other hand, for the high-density excitation, an efficient transport mechanism begins to function giving the wider spreading of the local exciton density. Then, it is expected that the lower the excitation density is reduced, the closer the spatial distributions of the local exciton density becomes to the luminescence distributions of the weak excitation limit. In fact, the peak shift distribution curve *c* for the lowest excitation in Fig. 5 is close to curve *d* in Fig. 11.

We have introduced two analogous parameters for the exciton dissipation processes: the decay length d in the energy-shift distribution on the pump-probe spectra, and the attenuation length ξ in the luminescence-intensity distribution. We have treated the decay length $d = \langle v \rangle \tau_{ex}$ as a function only of the excitation density I and not to depend on the coordinates r and spatially changing density n. This treatment is, of course, not accurate, because the dissipation rate depends not only on the initial excitation density but on the local exciton density n itself, and on the space coordinates implicitly through n. However, the fact that the simplified treatment reproduces well the experimental result implies that more heavily excited excitons transport themselves with higher efficiency resulting in the increase of d with increasing excitation density. Anyway, the length d is an index indicating the area in which the excitons at high density interact with each other.

On the other hand, the meaning of the attenuation length $\xi = v \tau_{ex}$ is relatively clear and quantitative. As already mentioned, our SFE system has a luminescence quantum efficiency of unity, giving only one decay mechanism on the luminescence intensity, i.e., the radiative decay process with the rate $1/\tau_{ex}$. Therefore, it can be said that excitons flow with one effective velocity in the area describable with an attenuation length.

In the first region fitting in the one flat line in Fig. 10, the velocity of the exciton flow has been evaluated to be close to the group velocity of the exciton polaritons for which any serious dephasing or slowing-down mechanisms do not operate. This region lengthens with increasing excitation density, and the length of the region is roughly equal to the quantity d for higher excitation densities; the index d indicates an area within which the excitons are at high density. It should be noted that the value $\xi = 2.3$ mm will be connected with the dissipation rate of such motion of the luminescent excitons around $k \simeq 0$, and does not correspond to the decay length d which exhibits the inverse of a gross dissipation rate of the total excitons along the expanding path. Then, it can be said that the high-density effect in this region is characterized by the reduction of the dissipation rate of the luminescent excitons, i.e., excitons at $k \simeq 0$. This suggests that the interaction of the high-density excitons brings about an increase in the coherency of the excitons around the band bottom. In addition, the increase of d with increasing excitation density would come from the increase in the contribution from the excitons in the coherent state.

In the second region of the other inclined line in Fig. 10, the exciton flow shows a different velocity with a smaller value exhibiting more frequent scattering or trapping processes. The obtained attenuation length $\xi \sim 0.17$ mm for the second region in curve *b* and curve *c* in the figure is close to the values 0.1–0.3 mm of the decay length d. Then, it is considered that, in such a region, the luminescent excitons begin to obey the same dissipation mechanism as that of the nonradiative excitons at $k \neq 0$. Thus, it is concluded that the higher density excitons bring about an increase in the number of excitons propagating coherently with the velocity near the exciton-polariton group velocity around the bottleneck. This suggests that a part of the high-density excitons are in an in-phase motion.

Concerning the conspicuous behavior of the SFE's at high density, i.e., the in-phase motion, we can get information on mean-free-path lengths of the excitons directly from the dephasing measurements on this exciton system. As mentioned in Sec. I, the time-of-flight measurements in this exciton system have given the average group velocity of exciton polariton $v_g \sim 6 \times 10^8$ cm/s for a low-density limit.[31] Besides, the dephasing time T_2 of the exciton state has been obtained to be more than ~ 10 ps even for the maximum excitation density in this work from the time correlated DFWM measurements.[32] From these values, the mean free path of the exciton $l_I (= v_g T_2)$ is evaluated to be ~ 60 μm in which the exciton is propagated without scattering. When we apply the drift velocity $\langle v \rangle \sim 1 \times 10^7$ cm/s instead of v_g from the pump-probe measurements as a velocity of excitons at high density, the mean free path l_I becomes at least ~ 1 μm.

The average exciton density $\bar{n} \simeq N_{abs}/\pi d^2$ is estimated to be $(5-8) \times 10^{12}$ cm^{-2} for every excitation density by using the value of the spatial decay length d on the assumption that all photons absorbed in the sample are transformed into excitons, N_{abs} being the absorbed photon number. This density provides an average distance between excitons to be ~ 40 Å, which should correspond to a mean-free-path length in a free

gas and is much shorter than the above-obtained values of the mean-free-path length l_I. Consequently, this result leads to the conclusion that the high-density excitons in this system must be in the in-phase collective motion without mutual collision.

Recent experiments concerning the Bose-Einstein condensation in excitonic gases provide some controversial discussion based on the spatial propagation of interacting boson systems in some new phase. For instance, in the phase of excitonic superfluidity, the exciton should be transported without attenuation as exemplified experimentally in Cu_2O.[18,19] As can be seen in Fig. 10, the spatial profiles of the heavily excited photoluminescence show the region growing with excitation density with very small attenuation. In such a region, the high-density effect bringing about the peak energy shift is remarkable, and the propagation velocity of the excitons is estimated to be comparable with the group velocity of the exciton-polariton mode. This characteristic spatial behavior of the high-density excitons or exciton-polaritons shows a possibility of a new phase of interacting exciton polaritons. Then, it is much more interesting to examine temporal behavior of our SFE's at high density in the real space. Space- and time-resolved spectroscopic experiments in the picosecond time domain are in progress in this system.

IV. CONCLUSION

We have observed directly the spatial propagation of SFE's at high density along the two-dimensional stacking disorder plane in BiI_3 applying the space-resolved spectroscopy methods. The intense laser excitation brings about significant change in the absorption spectra, i.e., blueshift and broadening, due to the interaction of the high-density excitons. The shift energy is proportional to the exciton density under the spatially uniform excitation condition. The space-resolved pump-probe absorption under high-density excitation also shows the spectral change even at the points more than 0.2 mm away from the exciting laser spot. The spatial distribution of the energy shift corresponding to the local exciton density was plotted as a function of distance r from the exciting position for various excitation densities. In this exciton system, the propagation mechanism is not characterized by diffusive one but by ballistic flow. From this fact, we adopted the high-density exciton flow in the two-dimensional space for the analysis of the energy shift distribution. The spatial distribution of the local exciton density can be well described by only a conveniently introduced parameter d, the decay length, for the exciton flow, which increases with increasing excitation density. For the maximum excitation density, the decay length gives the average velocity $\langle v \rangle$ of the exciton flow only one order of magnitude smaller than the group velocity v_g of an exciton-polariton mode observed in this system. Integrating the local exciton density estimated from the spectral shift over the whole area, we obtained the result that the total number of excitons is proportional to the net excitation density, i.e., net absorbed photon number per unit area. This result indicates that the decay time of the excitons in the whole area is constant and independent of the excitation density, although the distribution of excitons expands more with increasing excitation density. Accordingly, the average velocity, i.e., the drift velocity of the exciton flow, is to increase with increasing excitation density.

The luminescence spectra under the same intense laser excitation shows a similar change as in the pump-probe spectra accompanying the asymmetric tail to the low-energy side due to some relaxation processes. However, the space-resolved luminescence measurements give different spatial intensity distribution from that of the energy shift in the pump-probe spectra, although the integrated total luminescence intensity in the whole area is in proportion to the excitation density again as seen in the pump-probe spectra. The discrepancy between the two distributions comes from the difference of the number of excitons contributing to the luminescence process and the spectral shift; the former is represented by those around $k \simeq 0$ and occupies only a part of the total excitons, and the latter includes those in the total band region including $k \neq 0$ suffering any dissipation processes. We analyzed the luminescence intensity distribution on the basis of the two-dimensional exciton-polariton flow. From the decrease in the intensity with r, the two-step dissipation process was resolved by using the other parameter ξ, the attenuation length. In the first step region providing a larger value of ξ, the luminescent excitons flow with a very large velocity compared with the group velocity v_g. This area increases with increasing excitation density. In the second step region, the attenuation length ξ becomes close to the value of the decay length d, indicating the luminescent excitons to be governed by the same dissipation mechanism as on the total excitons in this region. The fact that the decay length d increases with increasing excitation density in the region with a large value of the attenuation length ξ suggests the existence of an in-phase motion in a new phase of the high-density SFE's. The in-phase motion was examined by estimating the mean-free-path lengths from the exciton density, the velocity of the exciton flow, and the dephasing time.

ACKNOWLEDGMENTS

We wish to thank Professor Takeshi Iida and Professor Masaki Aihara for valuable discussions on theoretical aspects. The help of Professor Teruo Komatsu and Dr. Taketoshi Kawai in the performing of experiments is also gratefully acknowledged. This work was supported by the Ministry of Education, Science, Culture and Sports of Japan under a Grant-in-Aid for Scientific Research.

*Present address: Department of Physics, Ehime University, Bunkyo-cho, Matsuyama 780, Japan.

[1] D. Fröhlich, A. Nöthe, and K. Reimann, Phys. Rev. Lett. **55**, 1335 (1985).

[2] G. W. Fehrenbach, W. Schäfer, J. Treusch, and R. G. Ulbrich, Phys. Rev. Lett. **49**, 1281 (1982).

[3] D. Hulin, A. Mysyrowicz, A. Antonetti, A. Migus, W. T. Masselink, H. Morkoç, H. M. Gibbs, and N. Peyghambarian, Phys. Rev. B **33**, 4389 (1986).

[4] K.-H. Schlaad, Ch. Weber, J. Cunningham, C. V. Hoof, G. Borghs, G. Weimann, W. Schlapp, H. Nickel, and C. Klingshirn, Phys. Rev. B **43**, 4268 (1991).

[5] S. Schmitt-Rink, D. S. Chemla, and D. A. B. Miller, Adv. Phys. **38**, 89 (1989).
[6] L. Schultheis, J. Kuhl, A. Honold, and C. W. Tu, Phys. Rev. Lett. **57**, 1635 (1986).
[7] D. P. Trauernicht and J. P. Wolfe, Phys. Rev. B **33**, 8506 (1986).
[8] H. Hillmer, A. Forchel, S. Hansmann, M. Morohashi, E. Lopez, H. P. Meier, and K. Ploog, Phys. Rev. B **39**, 10 901 (1989).
[9] Y. Takahashi, K. Muraki, S. Fukatsu, S. Kano, Y. Shiraki, and R. Ito, Jpn. J. Appl. Phys., Part 1 **32**, 5586 (1993).
[10] J. Hegarty, L. Goldner, and M. D. Sturge, Phys. Rev. B **30**, 7346 (1984).
[11] J. Hegarty and M. D. Sturge, J. Opt. Soc. Am. B **2**, 1143 (1985).
[12] L. M. Smith, J. S. Preston, J. P. Wolfe, D. R. Wake, J. Klem, T. Henderson, and H. Morkoç, Phys. Rev. B **39**, 1862 (1989).
[13] H. W. Yoon, D. R. Wake, J. P. Wolfe, and H. Morkoç, Phys. Rev. B **46**, 13 461 (1992).
[14] R. G. Ulbrich and G. W. Fehrenbach, Phys. Rev. Lett. **43**, 963 (1979).
[15] Y. Masumoto, Y. Unuma, Y. Tanaka, and S. Shionoya, J. Phys. Soc. Jpn. **47**, 1844 (1979).
[16] J. Aaviksoo, J. Lumin. **48&49**, 57 (1991).
[17] T. Reinot and J. Aaviksoo, J. Lumin. **50**, 259 (1991).
[18] E. Fortin, S. Fafard, and A. Mysyrowicz, Phys. Rev. Lett. **70**, 3951 (1993).
[19] E. Benson, E. Fortin, and A. Mysyrowicz, Phys. Status Solidi B **191**, 345 (1995).
[20] A. E. Bulatov and S. G. Tikhodeev, Phys. Rev. B **46**, 15 058 (1992).
[21] G. A. Kopelevich, S. G. Tikhodeev, and N. A. Gippius, Sov. Phys. JETP **82**, 1180 (1996).
[22] I. Loutsenko and D. Roubtsov, Phys. Rev. Lett. **78**, 3011 (1997).
[23] Y. Kaifu, J. Lumin. **42**, 61 (1988).
[24] T. Komatsu, Y. Kaifu, S. Takeyama, and N. Miura, Phys. Rev. Lett. **58**, 2259 (1987).
[25] T. Karasawa, T. Komatsu, and Y. Kaifu, Solid State Commun. **44**, 323 (1982).
[26] T. Komatsu, K. Koike, Y. Kaifu, S. Takeyama, K. Watanabe, and N. Miura, Phys. Rev. B **48**, 5095 (1993).
[27] T. Karasawa, T. Iida, M. Sakai, T. Komatsu, and Y. Kaifu, J. Phys. C **18**, 4043 (1985).
[28] I. Akai, T. Karasawa, Y. Kaifu, A. Nakamura, M. Shimura, and M. Hirai, J. Lumin. **42**, 357 (1989).
[29] I. Akai, T. Karasawa, T. Komatsu, and Y. Kaifu (unpublished).
[30] T. Kawai, I. Akai, and T. Karasawa, J. Phys. Soc. Jpn. **58**, 969 (1989).
[31] T. Kawai, S. Shimanuki, T. Karasawa, I. Akai, T. Iida, and T. Komatsu, J. Lumin. **48&49**, 721 (1991).
[32] M. Ichida, T. Karasawa, and T. Komatsu, Phys. Rev. B **47**, 1474 (1993).
[33] T. Karasawa, M. Ichida, I. Akai, and T. Komatsu, Appl. Phys. A: Solids Surf. **53**, 480 (1991).
[34] I. Akai, T. Karasawa, T. Komatsu, and Y. Kaifu, Phys. Rev. B **43**, 4484 (1991).
[35] I. Akai, T. Karasawa, and T. Komatsu, Int. J. Nonlinear Opt. Phys. **1**, 311 (1992).
[36] H. Kondo, T. Kawai, and T. Karasawa, Solid State Commun. **94**, 129 (1995).
[37] H. Kondo, T. Kawai, T. Karasawa, I. Akai, and T. Komatsu, J. Lumin. **66&67**, 448 (1996).
[38] T. Karasawa, I. Akai, T. Kawai, H. Kondo, H. Mino, and T. Komatsu, Prog. Cryst. Growth Charact. Mater. **33**, 97 (1996).
[39] K. Watanabe, T. Karasawa, T. Komatsu, and Y. Kaifu, J. Phys. Soc. Jpn. **55**, 897 (1986).
[40] E. Kato, T. Komatsu, and Y. Kaifu, J. Phys. Soc. Jpn. **54**, 3597 (1985).
[41] Y. Toyozawa, Prog. Theor. Phys. **20**, 53 (1958).
[42] To be exact, these spectral shapes should be fitted by the Voigt function in which certain inhomogeneous broadening including the slit width of the monochoromator is considered (Ref. 32). However, the significant difference was not recognized between the increase in the homogeneous broadening for heavy excitation obtained by the simple Lorentz function of Eq. (1) and that obtained by the Voigt function for these spectrum fittings in this work.
[43] The spatial distribution drawn in the figure is rather limited compared with the observed spectra. In practice, the integration was performed over the wider regions as much as observed.